

# Scaling Function Learning: A sparse aerodynamic data reconstruction method for generalizing aircraft shapes

Haitao Lin <sup>a</sup>, Xu Wang <sup>b</sup>, Weiwei Zhang <sup>a,c,d\*</sup>

*a. School of Aeronautics, Northwestern Polytechnical University, Xi'an 710072, China*

*b. Department of Mechanical Engineering, Hong Kong Polytechnic University, Hong Kong 999077*

*c. International Joint Institute of Intelligent Fluid Mechanics, Northwestern Polytechnical University, Xi'an 710072, China*

*d. National Key Laboratory of Aircraft Configuration Design, Xi'an 710072, China*

## Abstract

Accurate and complete aerodynamic data sets are the basis for comprehensive and accurate evaluation of the overall performance of aircraft. However, the sampling cost of full-state aerodynamic data is extremely high, and there are often differences between wind tunnel conditions and actual flight conditions. Conventional scaling parameter extraction methods can solve the problem of aerodynamic state extrapolation, but hard to achieve data migration and shape generalization. In order to realize the low-cost construction of a full-state nonlinear aerodynamic database, this research proposes the Scaling Function Learning (SFL) method, which mines the unified low-dimensional manifold of the aerodynamic force of aircraft with different shapes changing with the incoming flow state, thereby realizing nonlinear aerodynamic modeling with extremely small samples. In SFL method, symbolic regression is used to mine the composite function expression of aerodynamic force/moment coefficients for a relatively complete aerodynamic data set of typical aircraft. The inner layer of the composite function represents a scaling function, which has two key properties: 1) the architecture of the scaling function is universal to different shapes, allowing for generalization to various flow conditions by freezing constant terms; 2) the aerodynamic forces/moment coefficient is a weak nonlinear function of the correlation function, enabling accurate modeling with only a small number of samples. Therefore, the aerodynamic database for a new aircraft can be sparsely reconstructed and extrapolated across the full flight envelope with minimal data. The SFL method was validated on the HB-2 configuration by extracting scaling parameters for axial force coefficients and generalizing the scaling function by releasing its constants. The effectiveness and accuracy of the scaling function are verified using different hypersonic aircraft configurations, such as HBS, double ellipsoid, sharp cone, and double cone missile. The results show that the SFL method successfully achieves nonlinear dimensionality reduction of complex systems by extracting scaling parameters. The extracted scaling function has the ability to generalize across states and configurations. With only 3-4 state samples, the aerodynamic database construction of variable Mach number, angle of attack and Reynolds number can be realized, which shows great state extrapolation ability with a relative error of about 1-5%. The related research not only greatly reduces the aerodynamic acquisition cost of aircraft design, but also lays a methodological foundation for parameter space dimensionality reduction and small sample modeling of other complex high-dimensional engineering problems.

**Keywords:** Aerodynamic modeling; Scaling function; Nonlinear dimensionality reduction;

---

\* Corresponding author.

E-mail address: aeroelastic@nwpu.edu.cn (W. Zhang)

## 1. Introduction

During the design of the aircraft, obtaining comprehensive aerodynamic data across the entire flight envelope for different flow conditions is crucial for overall aerodynamic performance analysis and flight control law design. This requires extensive simulations and experiments. However, the sampling space for aerodynamic data is often high-dimensional and nonlinear, with parameters such as Mach number, Reynolds number, angle of attack, sideslip angle, rudder deflection angle, total enthalpy, and the wall-to-total temperature ratio influencing the aerodynamic characteristics. The cost of acquiring aerodynamic force data for all flow conditions within the flight envelope is extremely high. Moreover, aircraft design typically undergoes multiple rounds of iteration and optimization, further increasing the cost of generating aerodynamic data. Wind tunnel tests and simulations are also time-consuming. Reducing costs and improving efficiency have become urgent needs in the development of new aircraft.

In order to reduce the modeling sample requirements of high-dimensional and nonlinear aerodynamic data, data-driven methods have been widely used in the field of aerodynamic modeling. Brunton et al. [1] reviewed the research status of data-driven methods in the field of fluid mechanics, and gave important application prospects of data-driven methods such as deep neural networks, reduced-order models, and reinforcement learning in aerodynamic modeling, optimization, and control. Tang et al. [2] reviewed the application of machine learning methods in aerodynamic / thermal modeling, flow field prediction, transition / turbulence modeling, and prospected the development of intelligent aerodynamics. Zhang et al. [3] reviewed data-driven fluid dimensional analysis and intelligent scaling, flow feature extraction and dimensionality reduction, and systematically prospected the connotation and related research contents of intelligent fluid mechanics. Li et al. [4] carried out the transfer learning from two-dimensional airfoil to three-dimensional wing by embedding back-swept theory and using neural network. With 500 samples, they established a good aerodynamic model of a variable-shape three-dimensional wing. Wu et al. [5] used a generative adversarial network (GAN) to pre-train and fine-tune the airfoil flow field, achieving generalization of airfoils and flow conditions under sparse training data. Zhang & Peng [6] combined Kriging method and TCA dimension reduction method to make full use of concentrated load and distributed load to predict the concentrated force of airfoil under transonic and variable shape conditions. Pang et al. [7] used Landmark Affine ( LA ) to reduce the aerodynamic shape parameters to four, and realized efficient aerodynamic modeling and optimization of two-dimensional and three-dimensional aerodynamic shapes. The above data-driven black-box aerodynamic modeling method can achieve high-precision prediction of aerodynamic force within the state range of training data, and has certain generalization ability.

Although data-driven black-box models have made important progress in many fields, the physical interpretability and trustworthiness of existing black box models are not clear. When the predicted aerodynamic state range exceeds the training range, the credibility of the black box model to carry out aerodynamic data extrapolation is challenged. However, in practical engineering, because the cost of traversing all aerodynamic samples in the flight envelope is extremely high, the aerodynamic data is often incomplete, so aerodynamic prediction needs to be extrapolated.

Compared with the black-box data-driven method, the traditional scaling parameter method provides a more physical meaning for the variable state extrapolation of aerodynamic forces. Scaling parameters refer to dimensionless parameters that are combined based on theoretical derivation or expert experience to form future flow states. By scaling parameters, the aerodynamic characteristics under different incoming flow states can be aligned to the same function curve, thereby achieving effective extrapolation of aerodynamic characteristics under different aerodynamic conditions [8-10].

In the field of aerodynamics, the engineering application of scaling parameters can be traced back to the last century. In the flight test of the U.S. Space Shuttle, the ‘hypersonic anomaly’ phenomenon that the trim rudder angle is more than twice the design value occurs. The scaling parameter method is used to align ground data and flight data, in order to extrapolate ground data to predict flight data [10]. After decades of development, scaling parameters have been widely used in the scaling of hypersonic viscous interference effects, the scaling of aerodynamic heat, and the extrapolation of Reynolds number. Zhang et al. [11] established a viscous disturbance model of longitudinal aerodynamic coefficients under perfect gas conditions by combining the viscous disturbance parameter and the angle of attack as new scaling parameters. Khraibut et al. [12] proposed a scaling parameter composed of bluntness and angle of attack, in order to scale the pressure in the flow separation zone at different angles of attack in hypersonic flow. Sha et al. [13] used the modified viscous disturbance parameter and the normalized enthalpy difference  $Sw$  to scale the Stanton number  $St$  of the heat flow, so as to predict the heat flow on the surface of a hypersonic aircraft. Şakraker et al. [14] used the parameter  $KS$  and the parameter  $KH$  as the scaling parameters of the heat flux under supersonic and hypersonic conditions, respectively, so that the heat flux under different flow conditions can be calculated by a unified expression. Roncioni et al. [15] combined with numerical simulation and wind tunnel test, the Reynolds number extrapolation prediction of the aerodynamic force of the VEGA-C launch aircraft was realized by constructing a power law scaling parameter. Liu et al. [16] analyzed the relationship between shock wave position, shock front pressure and trailing edge pressure of supercritical airfoil by CFD simulation, and obtained the scaling parameters describing the influencing factors of Reynolds number effect. Özgören [17] achieved high Reynolds number extrapolation prediction of the aerodynamic polar lines of wind turbine airfoils by scaling parameters based on power laws.

In the above studies, the scaling parameters are mainly obtained by theoretical derivation and semi-empirical fitting based on numerical simulation, wind tunnel test or flight test data. Although these methods have theoretical support, they are still difficult to directly discover the scaling parameters through data without relying on prior knowledge, which makes the framework of scaling parameters largely depend on the quality of expert knowledge. In order to break through the limitations of prior knowledge and make the discovered scaling parameters more realistically reflect the physical characteristics of aerodynamic data, it is necessary to use data-driven white box modeling methods. Symbolic Regression (SR) is one of the suitable choices.

Symbolic regression is a supervised, interpretable white-box machine learning algorithm that mainly uses genetic programming to construct the expression that best fits the data set by selecting, mutating, and crossing over expression populations [18-21]. In terms of aerodynamic data scaling, many studies have used symbolic regression to extract scaling parameters. Luo et al. [8] proposed the Adaptive Space Transformation (AST) method to extract the scaling parameters of the axial force coefficient of a sharp cone at an angle of attack under hypersonic conditions, and used the

extracted scaling parameters to carry out extrapolation prediction, with better accuracy than Support Vector Machine (SVM) and neural network. Guo et al. [22] used symbolic regression to extract the scaling parameter of the blunting effect of the leading edge of the waverider to correlate the pressure increment caused by the blunting effect, thereby achieving efficient optimization of the waverider shape. Jiang et al. [23] proposed a Multi-space Interrelation theory to detect the invariants of aerodynamic data from different wind tunnels and achieve the correlation of the hypersonic heat flow Stanton number  $St$ . Ahmed et al. [24] used symbolic regression to extract the scaling parameters of the lift coefficient and drag coefficient of wind turbine blades for the stall delay performance of wind turbine blades, so as to accurately predict the aerodynamic performance of rotating blades at different wind speeds.

The existing scaling parameter extraction methods based on theoretical derivation or symbolic regression development, are limited to scaling and extrapolating the aerodynamic characteristics of different incoming flow conditions under a single or similar configuration. How to improve the generalization performance of scaling parameter expressions extracted by symbolic regression across different shapes and variable conditions is still a difficult problem in current research. Thus, this paper further generalizes the concept of scaling parameters to scaling functions. Compared with scaling parameters, scaling functions contain constant factors that change with specific aerodynamic shapes and require two properties: 1) the architecture of the scaling function is universal to different shapes, allowing for generalization to various flow conditions by freezing constant terms; 2) the aerodynamic forces/moment coefficient is a weak nonlinear function of the correlation function, enabling accurate modeling with only a small number of samples. The scaling function can fully leverage the aerodynamic data from historical configurations, enables cost reduction and efficiency improvements for the aerodynamic database of new aerodynamic shapes, and effectively extrapolates state parameters to predict aerodynamic performance at the boundary limits.

Focusing on the aerodynamic force/moment scaling across multiple shapes and a wide speed range in hypersonic regimes, this paper proposes a Scaling Function Learning (SFL) method in Section 2. The method involves two key steps: the extraction of scaling functions just from a typical aerodynamic configuration and the sparse reconstruction and parameter extrapolation for new configurations using these scaling functions. In Section 3, the SFL method is applied to a complete aerodynamic database of a typical configuration to extract a scaling function based on a combination of incoming flow condition. Four new configurations are used to validate the shape generalization, sparse reconstruction, and state extrapolation capabilities of the extracted scaling function. Section 4 concludes the paper and offers perspectives for future research.

## 2. Method

In this section, a framework for Scaling Function Learning (SFL) based on symbolic regression will be proposed. This approach extracts scaling parameter for aerodynamic forces/moment coefficient from a database of typical aerodynamic shapes. For new aerodynamic configurations, only a small number of aerodynamic samples are required to optimize the constant terms of the scaling parameter. By fitting the scaled quantities of these small samples with the optimized scaling parameters, an aerodynamic model for the new shape can be efficiently obtained.

As shown in Fig. 1, the proposed framework is divided into two parts: (a) extract the scaling function from typical aerodynamic shapes, and (b) use the extracted scaling functions to perform sparse reconstruction and parameter extrapolation of aerodynamic forces for new aircraft shapes. The detailed steps are as follows.

**Step 1:** The first part of the framework involves the extraction of scaling functions from typical aerodynamic shapes, as illustrated in Fig. 1(a). First, aerodynamic data is collected, including input aerodynamic state parameters  $(M, \alpha, \beta, Re, \delta, \dots)$  and output aerodynamic force/moment coefficients  $C$  for typical configurations. Here,  $M$ ,  $\alpha$ ,  $\beta$ ,  $Re$  and  $\delta$  represent the Mach number, angle of attack, sideslip angle, Reynolds number and rudder angle, respectively. Next, the aerodynamic state parameters are treated as independent variables, and the following mathematical operators are used: +, -,  $\times$ , /, square, and sqrt. A symbolic regression algorithm is then applied to initialize candidate scaling parameters  $S_i(M, \alpha, \dots)$ . In this step, the open-source PySR [21, 25, 26] framework for symbolic regression is used. PySR can efficiently find the best algebraic expression in the data according to the loss function. Considering that the scaled quantity  $C$  is a composite function  $C = f(S(M, \alpha, \beta, Re, \delta, \dots))$  of scaling parameters  $S$ , in order to make the scaling parameters have good generalization, the outer function  $f(\bullet)$  of the composite function should be a simple function with weak nonlinearity.  $f(\bullet)$  is assumed as a polynomial function. Therefore, the loss function for symbolic regression is set to be the MSE error of the polynomial fit of  $S$  to  $C$ :

$$loss = \frac{1}{n} \sum_{j=1}^n [C_{j, polyfit}(S_{i,j}, S_{i,j}^2, \dots) - C_j]^2 \quad (1)$$

In Eq. (1), the subscript  $j$  represents the  $j$ -th state sample of the typical aerodynamic shape,  $C_j$  represents the true value of the aerodynamic force/moment coefficient of the  $j$ -th aerodynamic sample, and  $C_{j, polyfit}(S_{i,j}, S_{i,j}^2, \dots)$  represents the predicted value of the polynomial fitting of the scaled quantity  $C_j$  with the  $j$ -th value of the  $i$ -th candidate scaling parameter expression  $S_{i,j}$ . Based on the value of the loss function, the symbolic regression algorithm performs selection, crossover, and mutation operations on the expressions, ultimately deriving the expressions  $S(M, \alpha, \beta, Re, \delta, \dots)$  for the scaling parameters of typical aerodynamic shapes. By releasing the constant terms  $(c_1, c_2, \dots)$  in the scaling parameters, these terms can vary across different shapes, effectively generalizing the scaling parameters into scaling functions  $S(M, \alpha, \beta, Re, \delta, \dots, c_1, c_2, \dots)$ . Unlike scaling parameters, scaling functions incorporate constant factors  $(c_1, c_2, \dots)$  that change with the specific aerodynamic configuration and are required to generalize across different shapes.

**Step 2:** The second part of the framework involves using the extracted scaling functions to perform sparse reconstruction and parameter extrapolation of aerodynamic forces for new aircraft shapes, as illustrated in Fig. 1(b). First, 3 or more aerodynamic state samples are selected within the flight envelope of the new shape, and the corresponding aerodynamic force/moment coefficients for the new configuration are obtained. Then, the constant terms  $(c_1, c_2, \dots)$  in the scaling functions  $S(M, \alpha, \beta, Re, \delta, \dots, c_1, c_2, \dots)$  are optimized based on these samples. The optimization objective is:

$$\min_{c_1, c_2, \dots} MSE = \frac{1}{n} \sum_{j=1}^n [C_{j, polyfit}(S_j(M, \alpha, \dots, c_1, c_2, \dots), S_j^2(M, \alpha, \dots, c_1, c_2, \dots), \dots) - C_j]^2 \quad (2)$$

The polynomial degree of Eq. (2) is consistent with that of Eq. (1). The Eq. (2) is optimized

with the small sample data of the new shape. The optimization method adopts the Nelder-Mead algorithm to obtain the scaling parameter expression  $S'(M, \alpha, \beta, Re, \delta, \dots, c_1', c_2', \dots)$  after optimizing the constant term, and use  $S'$  to perform polynomial fitting on the small sample aerodynamic data of the new shape. The polynomial degree is consistent with Eq. (1) and Eq. (2), and the polynomial expression of the force/moment coefficient  $C = C(S', S'^2, \dots)$  corresponding to the new shape can be obtained, so as to complete the sparse reconstruction and parameter extrapolation of the aerodynamic force of the new shape. The specific algorithm is shown in **Algorithm 1**.

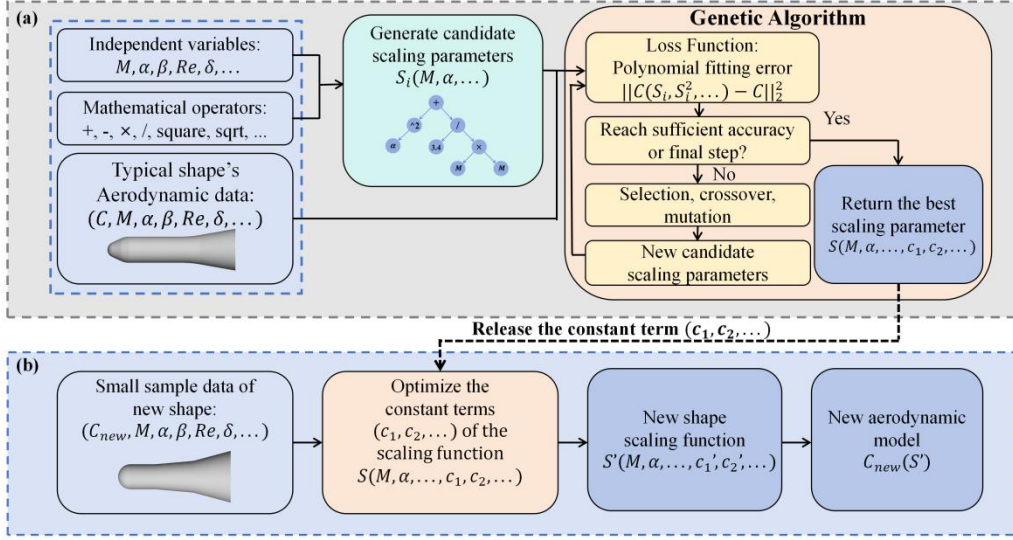


**Fig. 1.** SFL method framework: (a) Scaling function extraction and (b) Sparse reconstruction of aerodynamic forces for new shapes based on the extracted scaling parameters.

---

**Algorithm 1: Scaling Function Extraction and Aerodynamic Modeling.**

---

**Input:** Aerodynamic data of typical aerodynamic shapes (state parameters  $(M, \alpha, \beta, Re, \delta, \dots)$ , force/moment coefficients  $C$ ), new shape's aerodynamic data  $(C_{new}, M, \alpha, \beta, Re, \delta, \dots)$  (small sample).

**Output:** Scaling function expression, aerodynamic force/moment polynomial expression for the new shape.

**Step 1: Scaling Function Extraction from typical shape's aerodynamic data.**

- 1: Initialize the Symbolic regression algorithm (PySR) with operators: +, -,  $\times$ , /, square, sqrt.
- 2: Take the aerodynamic state parameters  $(M, \alpha, \beta, Re, \delta, \dots)$  and the associated force/moment coefficients  $C$  of the typical shape as inputs for symbolic regression.
- 3: Use symbolic regression to generate candidate scaling parameters  $S_i(M, \alpha, \beta, Re, \delta, \dots)$ .
- 4:  $step \leftarrow 0$
- 5: **while**  $step < step_{max}$  **do**
- 6:     Calculate the loss function (Eq. (1)) of each candidate scaling parameters.
- 7:     **if not** reach sufficient accuracy **then**

- 8: Perform selection, crossover, and mutation of expressions.
- 9: Update candidate scaling function expressions.
- 10:  $step \leftarrow step + 1$
- 11: **else**
- 12: **return** the best scaling parameter expression  $S(M, \alpha, \beta, Re, \delta, \dots)$  .
- 13: Release the constant term of the scaling parameters to obtain the scaling function  $S(M, \alpha, \beta, Re, \delta, \dots, c_1, c_2, \dots)$ .

### Step 2: Small sample aerodynamic modeling for a new shape.

- 1: Take the new shape aerodynamic data  $(C_{new}, M, \alpha, \beta, Re, \delta, \dots)$  as inputs.
  - 2: Optimize the constant terms  $(c_1, c_2, \dots)$  of the extracted scaling function expression  $S(M, \alpha, \beta, Re, \delta, \dots, c_1, c_2, \dots)$  using the Nelder-Mead algorithm. The optimization objective is to minimize the polynomial fitting mean absolute error of  $C_{new}(S')$  (Eq.(2) ). The polynomial degree of Eq.(2) is consistent with Eq. (1).
  - 3: Obtain the optimized scaling function  $S'(M, \alpha, \beta, Re, \delta, \dots, c_1', c_2', \dots)$ .
  - 4: Polynomial fit the small sample force/moment coefficient  $C_{new}$  using the scaling parameter  $S'$  to obtain the force/moment coefficient expression  $C_{new}(S')$  for the new shape.
- 

## 3. Case Validation and Result Analysis

To verify the ability of the Scaling Function Learning (SFL) method to extract aerodynamic scaling functions and its generalization capability, the HB-2 is selected as a representative aerodynamic shape. A comprehensive aerodynamic database for HB-2 will be obtained through CFD simulations, and the axial force scaling function was extracted using the method described in Section 2. Subsequently, we will test the scaling function's generalization to different shapes and its ability for sparse reconstruction and extrapolation with limited samples using CFD data from HBS, double ellipsoid, sharp cone, and double cone missile configurations. The range of CFD simulation states for each shape is covered  $1.5 < M < 10, -20^\circ < \alpha < 20^\circ, 10^4 < Re < 3 \times 10^6$  comprehensively. To ensure the accuracy of the aerodynamic data, the CFD solver will be validated first.

### 3.1 CFD Solver Validation

The HB-2 configuration [27, 28] is a hypersonic shape with a blunt cone forebody, a cylindrical midsection, and an aft expansion skirt. Its geometry and computational grid are shown in Figure 2. The aerodynamic database for HB-2 was obtained using the CFD method, with the CFD solver being the NNW-FlowStar software and the turbulence model set to SST.

Fig. 3 compares the CFD-calculated axial and normal force coefficients of the HB-2 at given states  $M = 8, \alpha = 0, 2^\circ, 4^\circ, 6^\circ, 8^\circ, 10^\circ, 12^\circ$  with the wind tunnel test data from FD-7 [29]. The CFD results closely match the experimental data, with relative errors of 0.89% for the axial force coefficient and 1.69% for the normal force coefficient, demonstrating the accuracy of the CFD calculations in predicting aerodynamic coefficients. The relative error formula used in this paper is as follows:

$$Relative\ Error = \frac{\sum_{i=1}^n |C_{i,pre} - C_i|}{\sum_{i=1}^n |C_i|} \quad (3)$$

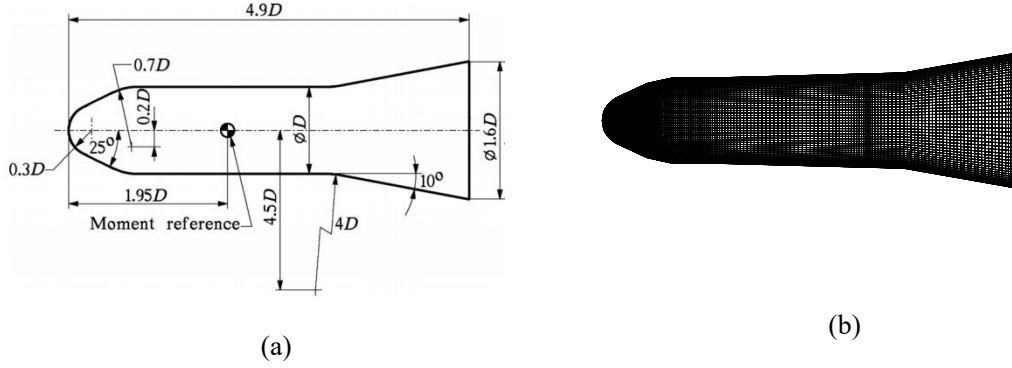


Fig. 2. (a) Geometry<sup>[28]</sup> and (b) Computational grid of HB-2.

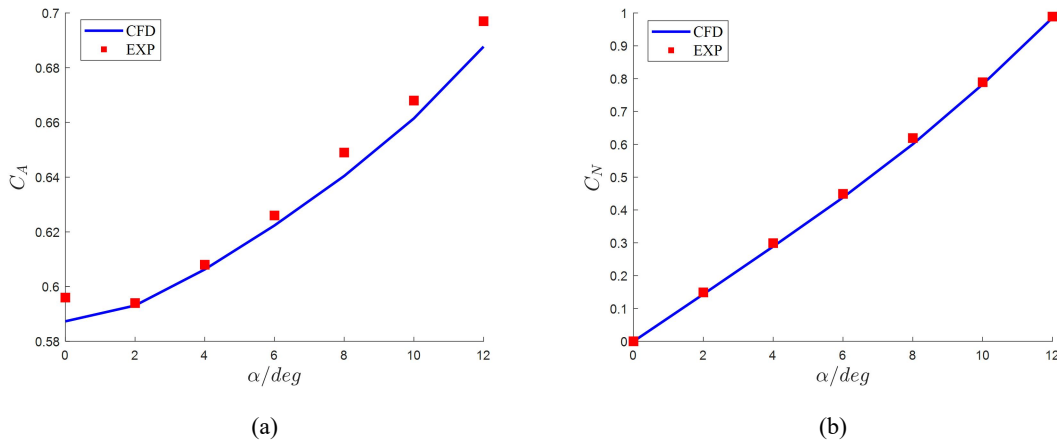


Fig. 3. CFD solver validation: (a) Axial force coefficient from CFD and wind tunnel experiments at  $M=8$  and (b) Normal force coefficient from CFD and wind tunnel experiments at  $M=8$ .

### 3.2 Extraction of Axial Force Scaling Parameters for HB-2

To extract the axial force scaling parameters for HB-2, a comprehensive aerodynamic database must first be obtained through CFD simulations. The simulation states were selected using Latin hypercube sampling [30], covering a range of  $1.5 < M < 10$ ,  $-25^\circ < \alpha < 25^\circ$ ,  $10^4 < Re < 3 \times 10^6$ , where  $M$  represents the Mach number,  $\alpha$  represents the angle of attack, and  $Re$  represents the Reynolds number, with the sideslip angle fixed at zero. A total of 100 sample points were calculated, with the ratio of state quantities for  $\alpha = 0$ ,  $0 < |\alpha| < 10^\circ$ , and  $10^\circ < |\alpha| < 25^\circ$  being approximately 1:2:2. Using the CFD results, a complete aerodynamic database for HB-2 was established. The distribution of the axial force coefficient  $C_A$  as a function of  $M$  and  $\alpha$  is shown in Fig. 4.

The scaling parameter extraction method based on symbolic regression proposed in Section 2 is used to extract the axial force scaling parameter of HB-2. The number of iterations of the symbolic

regression algorithm is set to  $\text{step}_{\max}=1500$ , the sufficient accuracy is set to  $1e-8$ , and the polynomial order in the loss function is set to 2. The axial force coefficient scaling parameters  $S_A$  obtained are as follows (the angle unit is rad):

$$S_A = \left( \alpha^2 + \frac{3.38}{M^2} \right) \sqrt{M} \quad (4)$$

In Eq.(4), the physical significance of each scaling parameter is as follows:  $\alpha^2$  is related to lift-induced drag,  $\frac{3.38}{M^2}$  is associated with wave drag and base drag, and the constant 3.08 represents a quantity linked to geometric shape. By utilizing the extracted axial force scaling parameter expression  $S_A$ , the axial force coefficients  $C_A$  under different Mach numbers and angles of attack can be scaled onto a second-order polynomial curve  $C_A(S_A)$ , as shown in Fig. 5. Since the relationship between  $S_A$  and  $M$  is not linear, and the sampled Mach numbers are approximately evenly distributed, more data points are concentrated in the lower  $S_A$  range.

From the scaling parameter expression in Eq.(4), it can be seen that after the transformation, the influence of Mach number and angle of attack on the axial force coefficient is captured through the scaling parameters  $S_A(M, \alpha)$ . This effectively reduces the dimensionality of the nonlinear relationship of  $(C_A, M, \alpha)$ . Fig. 6 shows a set of contour lines of  $S_A$  under different flow conditions  $(M, \alpha)$ , representing the low-dimensional manifold corresponding to the scaling parameters. Along the same contour line, no matter how  $(M, \alpha)$  change, the values of the scaling parameters  $S_A$  and the axial force coefficient  $C_A$  remain constant.

Using the isovalue relationship characterized by the scaling parameters, obtaining the axial force coefficient for just one state on a contour line is equivalent to knowing the axial force coefficients for all points along that contour. This enables the scaling parameters to achieve extrapolation across different flow conditions. Based on this principle, the data for a single angle of attack ( $\alpha = 0$ ) was used as the training set to fit a second-order polynomial of  $C_A(S_A)$ , and tested it with the data of  $0 < |\alpha| < 25^\circ$ . The relative error for the test set was only 1.46%, confirming the capability of the scaling parameters to extrapolate across different flow conditions.

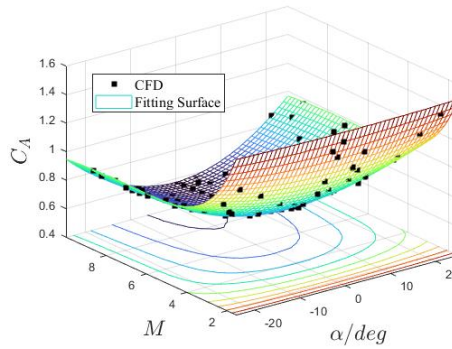
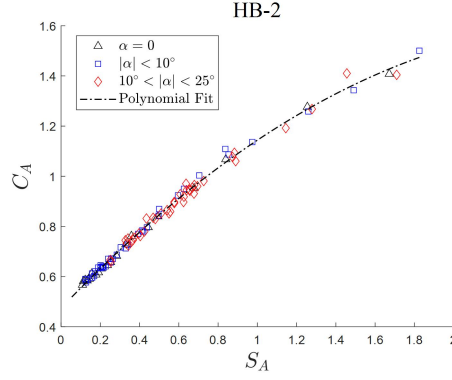
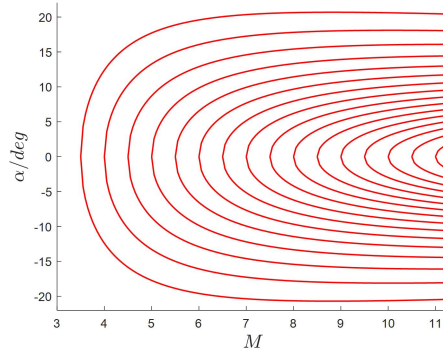


Fig. 4. Distribution of axial force coefficient  $C_A$  for HB-2.



**Fig. 5.** Distribution of axial force coefficient  $C_A(S_A)$  for HB-2.



**Fig. 6.** Contour of the scaling parameters  $S_A$ .

### 3.3 Identification and Validation of the Scaling Function for Shape

#### Generalization

In the previous section, we extracted the axial force scaling parameters for the HB-2 shape and verified their generalization ability in the state space and their extrapolation capability. In this section, the scaling parameter will be extended to scaling function, and the CFD aerodynamic databases for the HBS [31], double ellipsoid [32], sharp cone ( $10^\circ$  half-angle) [33], and double cone missile [34] will be used to further validate the shape generalization performance of the scaling function.

The CFD databases for the HBS, double ellipsoid, sharp cone ( $10^\circ$  half-angle) and double cone missile configurations were calculated, with the aerodynamic shapes shown in Fig. 7. The range of flow conditions considered was:  $1.5 < M < 10$ ,  $-20^\circ < \alpha < 20^\circ$ ,  $10^4 < Re < 3 \times 10^6$ , with the ratio of state quantities for  $\alpha = 0$ ,  $0 < |\alpha| < 10^\circ$ , and  $10^\circ < |\alpha| < 20^\circ$  being approximately 1:2:1.5.

Next, a step-by-step approach will be adopted, carefully considering the geometric characteristics of each aerodynamic shape and their corresponding aerodynamic properties, to progressively relax the constant terms in Eq.(4) and obtain a scaling function that is generalizable

across different shapes. Subsequently, the shape generalization performance of the scaling function will be verified using aerodynamic data from various configurations. It is important to note that for the same shape, the constant terms of the scaling function are fixed, but for different shapes, the constant terms can be optimized based on the specific aerodynamic characteristics of each shape.

First, the constant term  $c_1$  of the scaling parameter in Eq.(4) was released and generalized to:

$$S_A = (\alpha^2 + \frac{c_1}{M^2})\sqrt{M} \quad (5)$$

Next, it was observed from the  $\alpha^2$  term in Eq. (5) that the corresponding values of  $S_A$  are equal for  $\pm\alpha$ , and the corresponding values of  $C_A$  are also equal for  $\pm\alpha$ . This isovalue relationship holds only when the shape is symmetric about the horizontal plane. Therefore, Eq.(5) represents a special case for shapes that are horizontally symmetric. To apply this to asymmetric shapes, it can be further generalized as:

$$S_A = ((\alpha - \alpha_0)^2 + \frac{c_1}{M^2})\sqrt{M} \quad (6)$$

In Eq.(6), for symmetric shapes,  $\alpha_0 = 0$ , while for asymmetric shapes,  $\alpha_0 \neq 0$ .

Eq.(6) is a universal scaling function for blunt body shapes. To prove this view, according to the method of Step 2 in Part 2, the undetermined parameters  $c_1$  and  $\alpha_0$  in Eq.(6) were optimized using partial aerodynamic data of HBS and double ellipsoid. The optimized  $S_A$  was used to establish the second-order polynomial  $C_A(S_A)$ , and the fitting error was evaluated using the test set. For the HBS configuration, since  $\alpha_0 = 0$ ,  $c_1$  was optimized using only the data of  $\alpha = 0$  as the training set. After optimization,  $c_1 = 2.30$  was obtained, and the distribution of  $C_A(S_A)$  is shown in Fig. 8(a), where the relative error of the test set is 2.10%. For the double ellipsoid configuration,  $c_1$  and  $\alpha_0$  were optimized using the data of  $|\alpha| < 10^\circ$  as the training set. After optimization,  $c_1 = 3.21$  and  $\alpha_0 = 0.162rad$  was obtained, and the distribution of  $C_A(S_A)$  is shown in Fig. 8(b), where the relative error of the test set is 2.21%.

However, when the axial force coefficient of the  $10^\circ$  half-angle sharp cone was correlated using Eq.(6), it was found that the resulting expression exhibited significant error due to the fact that Eq.(6) does not account for the effects of Reynolds number. This is because the sharp cone is a pointed-body shape, and its boundary layer thickness is thinner than that of blunt-body shapes, making its axial force coefficient more sensitive to changes in Reynolds number. Therefore, by using aerodynamic data for the sharp cone configuration and incorporating the Reynolds number effects, Equation (6) is further generalized as:

$$S_A = ((\alpha - \alpha_0)^2 + \frac{c_1}{M^2})\sqrt{M} \times (\log_{10} Re)^{c_2} \quad (7)$$

For the sharp cone configuration,  $\alpha_0 = 0$ , only the  $\alpha = 0$  data were used as the training set, and the optimization yielded  $c_1 = 3.09$ ,  $c_2 = -0.68$ . The distribution of  $C_A(S_A)$  is shown in Fig. 8(c), and the relative error for the test set is 4.44%.

Regardless of whether the configuration is a pointed body or a blunt body, the axial force coefficient can be related by Eq.(7). The scaling function in Eq.(7) was then validated using aerodynamic data from the double cone missile shape. Using the data of  $\alpha = 0$  for the double cone missile configuration as the training set, and based on symmetry,  $\alpha_0 = 0$ , the optimization

yielded  $c_1 = 3.10$ ,  $c_2 = -0.68$ . The distribution of  $C_A(S_A)$  is shown in Fig. 8(d), and the relative error for the test set is only 1.48%.

Table 1 presents the optimized values of  $c_1$ ,  $\alpha_0$  and  $c_2$ , along with the relative error of  $C_A(S_A)$  on the test set, for different aerodynamic shapes when the training set consists of  $\alpha = 0$  (symmetric configuration) or  $|\alpha| < 10^\circ$  (asymmetric configuration).

By considering the geometric characteristics of different shapes and their corresponding aerodynamic properties, the constant terms in the scaling parameters of Eq.(4) were progressively released. This ultimately led to the development of a generalizable scaling function, given by Eq.(7), which can scale the axial force coefficients of different aerodynamic shapes across various states to a second-order polynomial curve, with a relative error ranging from 1% to 4%. Thus, the generalization and extrapolation capabilities of the scaling function in Eq.(7) for different shapes and states have been validated.

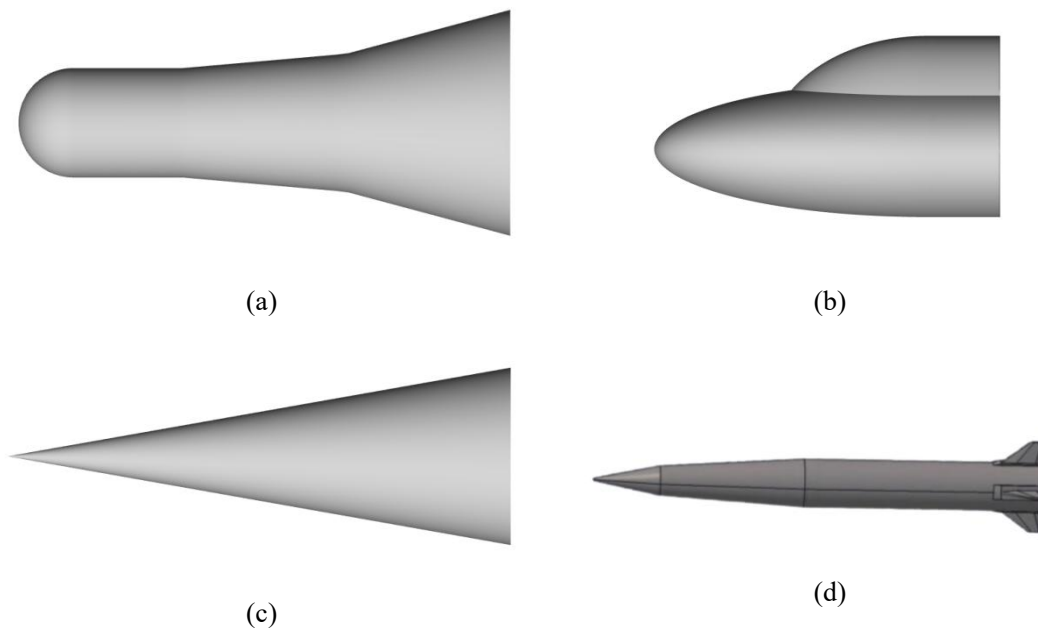
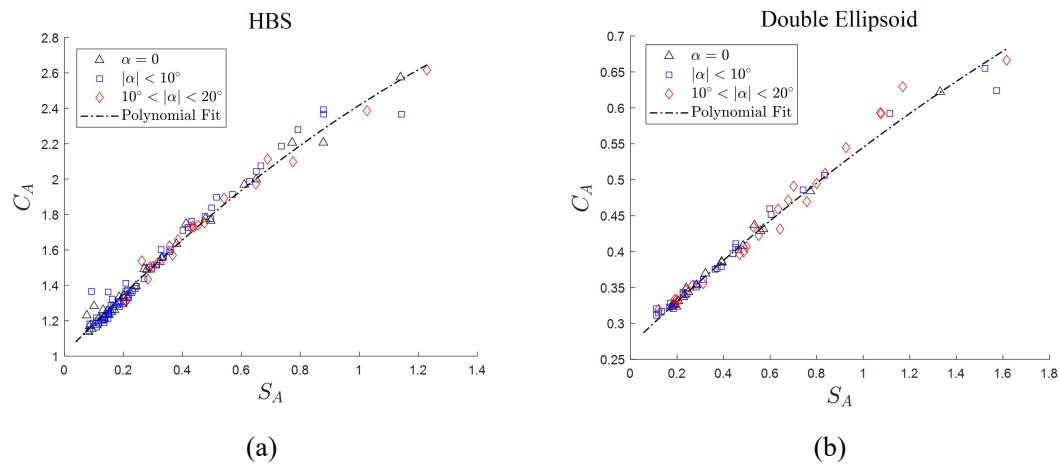
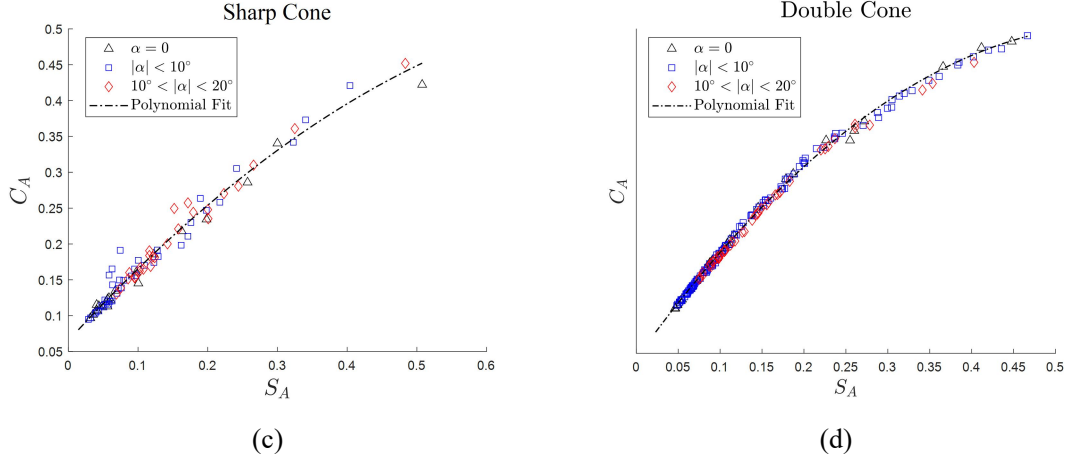


Fig. 7. Aerodynamic shapes of (a) HBS, (b) double ellipsoid, (c) sharp cone ( $10^\circ$  half-angle), and (d) double cone missile [34].





**Fig. 8.** Comparison between scaling function modeling and CFD data when the training set is  $\alpha = 0$  (for symmetric configurations) or  $|\alpha| < 10^\circ$  (for asymmetric configurations): (a) HBS, (b) double ellipsoid, (c) sharp cone (half-angle), and (d) double cone missile.

**Table 1.** Optimized  $c_1$ ,  $\alpha_0$ , and  $c_2$  for different aerodynamic shapes when the training set is  $\alpha = 0$  (for symmetric configurations) or  $|\alpha| < 10^\circ$  (for asymmetric configurations), along with the relative error of  $C_A(S_A)$  on the test set.

Aerodynamic Shapes	$c_1$	$\alpha_0 / \text{rad}$	$c_2$	Relative Error
HBS	2.30	0	0	2.10%
Double Ellipsoid	3.21	0.162	0	2.21%
Sharp Cone	3.09	0	-0.68	4.44%
Double Cone Missile	3.10	0	-0.68	1.48%

### 3.4 Sparse Reconstruction of Axial Force Coefficient Using Scaling Functions

To fully leverage the extrapolation and generalization capability of the scaling function across different shapes and states, we aim to achieve a sparse reconstruction of the axial force coefficient for various aerodynamic configurations within the smallest possible state range and using the fewest possible samples. This approach significantly reduces the cost of aerodynamic data acquisition in aircraft design. According to Step 2 in Section 2, we will select 3 to 4 aerodynamic samples within the state space  $M < 5$  to serve as the training set. These samples will be used to optimize the parameters in the scaling function, and the optimized scaling function, combined with these samples, will be used to construct a full-state aerodynamic model  $C_A(S_A)$ .

According to Section 3.3, the axial force coefficient of blunt bodies is minimally affected by the Reynolds number, the parameter  $c_2$  associated with the Reynolds number in the blunt body is set to  $c_2 = 0$ . Additionally, for symmetric shapes,  $\alpha_0 = 0$  applies. Therefore, for the blunt symmetric shapes HB-2 and HBS, only  $c_1$  in Equation (7) needs to be optimized. In contrast, for the double ellipsoid shape, both  $c_1$  and  $\alpha_0$  require optimization. Similarly, for the sharp cone and double cone missile shapes,  $c_1$  and  $c_2$  need to be optimized. The number of training

samples chosen for HB-2, HBS, double ellipsoid, sharp cone, and double cone missile shapes are 3, 3, 4, 4, and 4, respectively. **Table 2** provides the sampling conditions for sparse aerodynamic reconstruction and the range of conditions for the test set. The Mach number range for the training samples is  $1.5 < M < 5$ . For symmetric configurations, the range of angles of attack in the training set is  $\alpha = 0$ . For the asymmetric double ellipsoid configuration, the angle of attack range in the training set is  $|\alpha| < 10^\circ$ , which ensures sufficient optimization of the parameter  $\alpha_0$ .

**Table 2.** Range of flow conditions for training and test sets in small-sample sparse reconstruction.

Flow Parameters	Training Set (3-4 samples)	Test Set
M	$1.5 < M < 5$ , with samples selected uniformly	$1.5 < M < 10$
$\alpha$	$\alpha = 0$ (symmetric configurations) or $ \alpha  < 10^\circ$ (asymmetric configurations)	$-20^\circ < \alpha < 20^\circ$
Re	$10^4 < Re < 3 \times 10^6$	$10^4 < Re < 3 \times 10^6$

The sparse reconstruction results for the axial force coefficients of various shapes are shown in **Fig. 9**. The stars represent the aerodynamic samples in the training set, while the dashed line represents the second-order polynomial curve  $C_A(S_A)$  obtained from sparse reconstruction using a small number of samples. The scatter points correspond to the CFD data from both the training and test sets. It was observed that, although a few aerodynamic data points at large angles of attack deviate from the  $C_A(S_A)$  curve, the overall relative error of the full-state aerodynamic database, built using only 3 to 4 aerodynamic samples, remains within 1-5%. **Table 3** presents the optimized  $c_1$  and  $\alpha_0$ , as well as the relative error from the sparse reconstruction modeling with limited samples.

**Fig. 10** illustrates the probability distribution of relative error for the test set during the sparse reconstruction of the axial force coefficients for each shape. It can be seen that the relative errors of the test set data points are concentrated in the range of 0-4%.

These results demonstrate that, by utilizing the scaling parameter framework for typical shapes, sparse reconstruction of aerodynamic databases for new shapes can be achieved with as few as three aerodynamic samples. This method allows for sparse reconstruction based on CFD simulations, wind tunnel experiments, or flight tests across different shapes, with flow conditions covering  $1.5 < M < 11, |\alpha| < 20^\circ, 10^4 < Re < 3 \times 10^6$ .

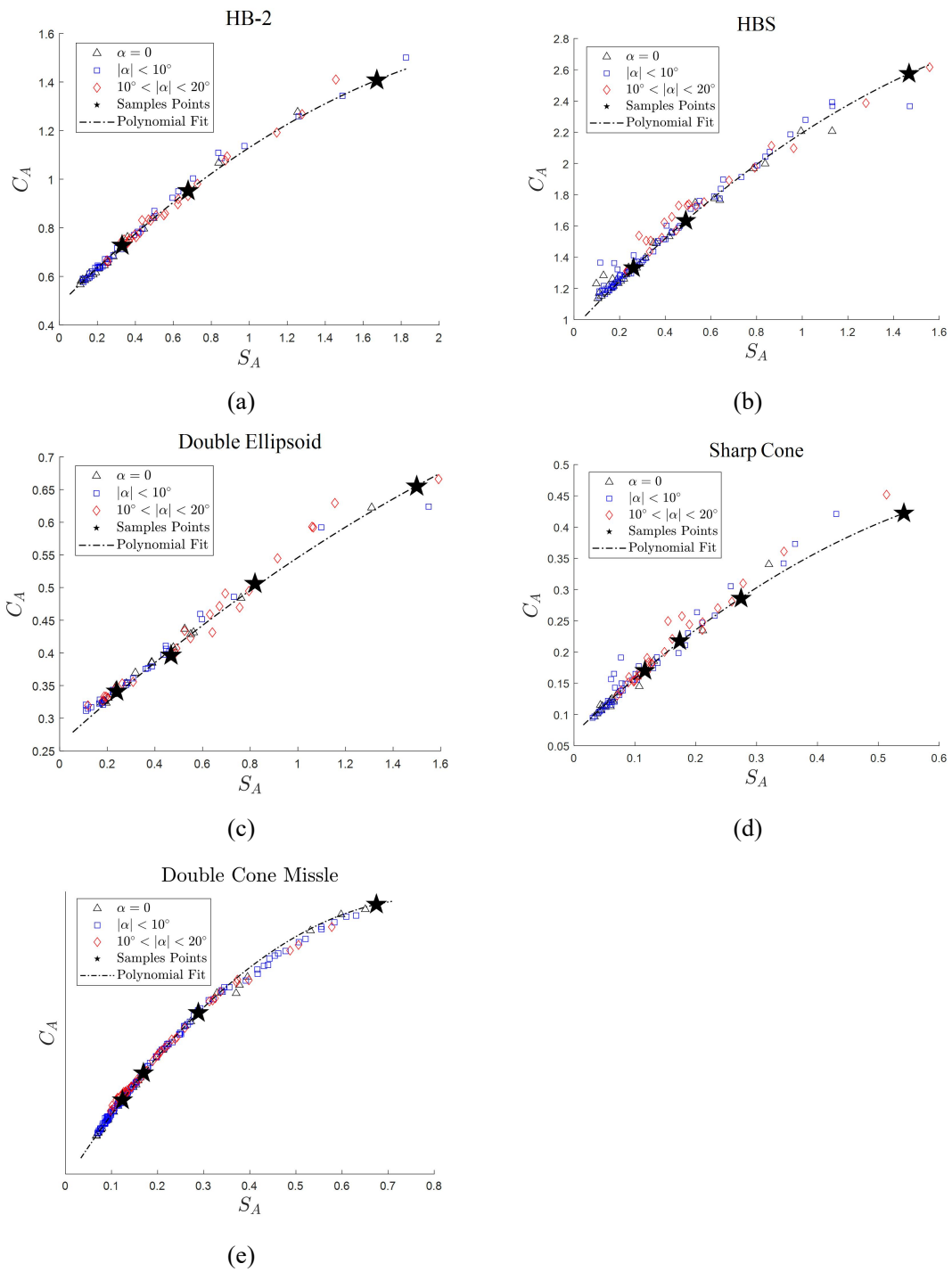


**Fig. 9.** Results of axial force coefficient modeling using 3 samples: (a) HB-2, (b) HBS, (c) double ellipsoid, (d) sharp cone ( $10^\circ$  half-angle), and (e) double cone missiles. The stars represent training samples, and the dashed lines represent aerodynamic models built using 3-4 samples.

**Table 3.** Optimized parameters and relative error on the test set for different aerodynamic shapes, during sparse reconstruction of axial force coefficients using 3-4 samples.

Aerodynamic Shapes	$c_1$	$\alpha_0$ /rad	$c_2$	Relative Error
HB-2	3.08	0	0	1.77%
HBS	2.96	0	0	2.46%
Double Ellipsoid	3.16	0.16	0	2.64%
Sharp Cone	3.30	0	-0.68	5.15%
Double Cone	4.50	0	-0.67	1.68%
Missile				

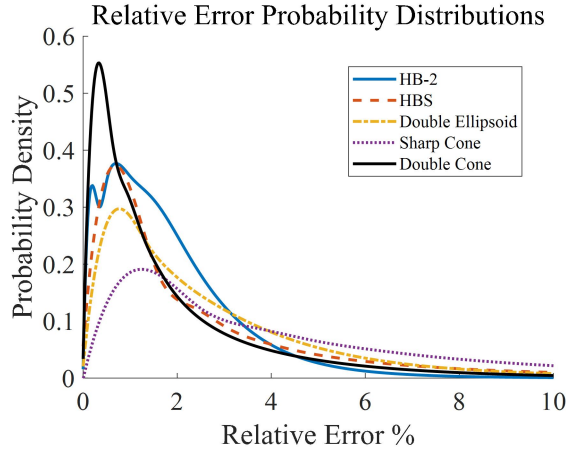


**Fig. 10.** Probability distributions of relative error in the test set for axial force coefficient sparse reconstruction using small samples with the SFL method.

To further compare the extrapolation capabilities of the Scaling Function Learning (SFL) method and black-box machine learning models, a Kriging model was also employed to model and extrapolate the axial force coefficients for the HB-2, HBS, double ellipsoid, sharp cone, and double cone missile shapes.  $(\alpha, M, \log_{10} Re)$  were used as inputs to the Kriging model, and  $C_A$  as outputs. All aerodynamic data from  $M < 5$  were used as the training set for the Kriging model (as training with only three samples was not feasible due to insufficient data), while the remaining  $M > 5$  were used as the test set to evaluate the extrapolation performance.

**Fig. 11(a)** and **Fig. 11(b)** show the modeling and extrapolation results for the axial force coefficients of the HB-2 shape using the SFL and Kriging methods, with relative errors on the test set of 1.77% and 75.67%, respectively. Although the SFL method used only 3 training samples, significantly fewer than the 38 samples used by the Kriging model, its extrapolation accuracy was far superior to that of the Kriging model. Additionally, **Fig. 11(c)** and **Fig. 11(d)** present a comparison of the axial force coefficient contours obtained by the SFL and Kriging methods against reference contours. The reference contours were derived from augmented aerodynamic data using a neural network. Due to the constraints imposed by the scaling function framework, the aerodynamic database obtained through sparse reconstruction using the SFL method yielded

contours that closely matched the reference contours. In contrast, the contours predicted by the Kriging model deviated substantially from the reference during extrapolation, highlighting the significant superiority of the SFL method for aerodynamic state extrapolation. **Table 4** presents the relative errors on the test sets for all shapes, comparing the performance of the SFL and Kriging methods.

This section demonstrates that small-sample modeling using the SFL method can effectively build aerodynamic databases for new shapes within the framework of typical shape scaling parameters. With as few as 3-4 aerodynamic samples, CFD calculations, wind tunnel experiments, or flight test data for different shapes can be sparsely reconstructed, covering flow conditions within the range of  $1.5 < M < 10, |\alpha| < 20^\circ$ . The results of small-sample scaling modeling and extrapolation further confirm the strong generalization and extrapolation capabilities of this scaling parameter framework under varying shape and flight conditions. This highlights that scaling parameters can serve as a powerful tool for reducing costs and improving efficiency in aerodynamic testing.

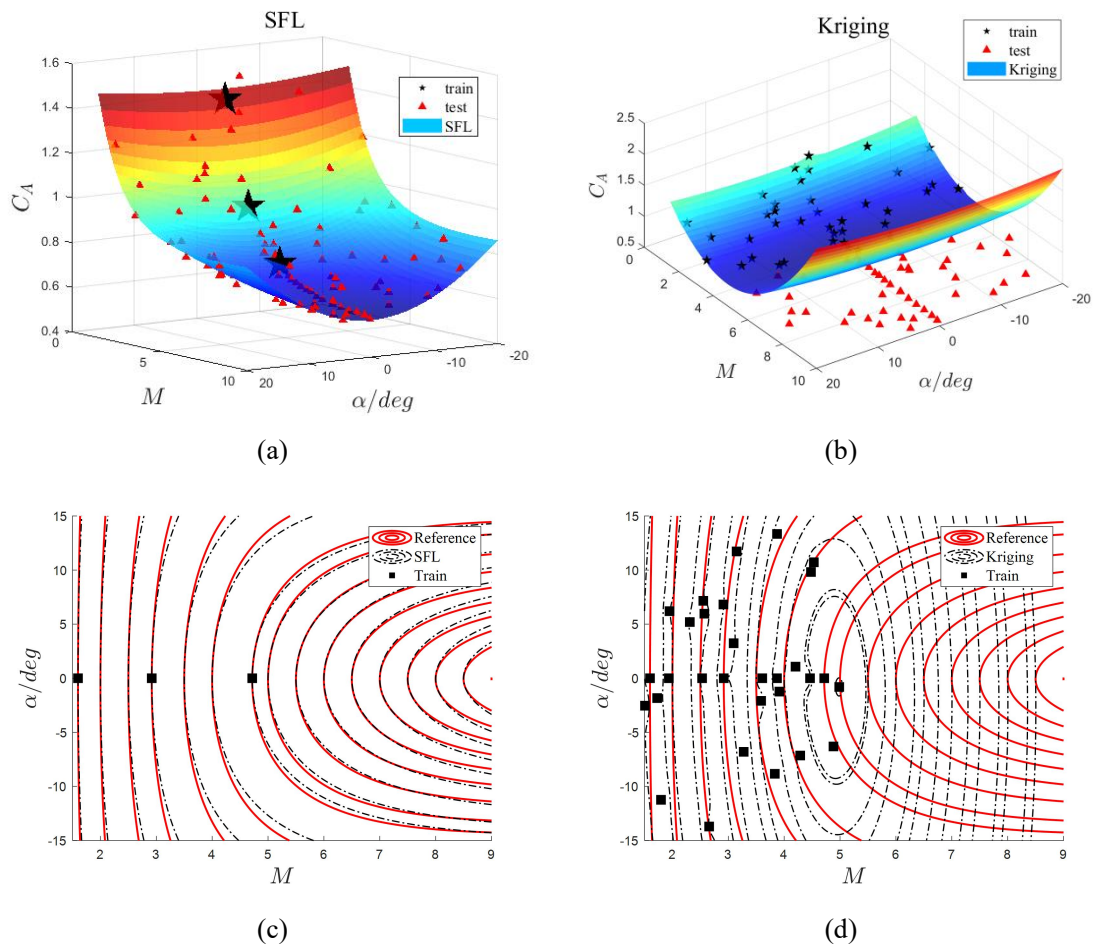


**Fig. 11.** State extrapolation of axial force coefficients for the HB-2 shape using (a) the SFL method (with only 3 samples in the training set) and (b) the Kriging method (with 38 samples in the training set). (c) and (d) show the comparison of contour lines obtained by the SFL and Kriging methods with reference contour lines, where the reference contour lines were extracted from augmented aerodynamic data using a neural network.

**Table 4.** Comparison of relative errors in extrapolation predictions between the SFL and Kriging methods.

	Relative Error (SFL)	Relative Error (Kriging)
HB-2	1.77%	75.67%
HBS	2.46%	44.71%
Double Ellipsoid	2.64%	38.36%
Sharp Cone	5.15%	76.71%
Double Cone Missile	1.68%	44.86%

## 4. Conclusions

To effectively leverage historical aerodynamic data from existing aircraft shapes, reduce the aerodynamic sample requirements for new shape designs, and achieve low-cost construction of full-state nonlinear aerodynamic databases for various shapes, this paper extends scaling parameters into scaling functions and proposes a Scaling Function Learning (SFL) method. In the SFL approach, the loss function of symbolic regression is set to minimize the polynomial fitting error of candidate scaling function expressions to the scaled quantity, enabling the extraction of scaling parameters from the comprehensive aerodynamic databases of typical aircraft. By releasing the constant terms in the scaling parameter, the resulting scaling function can achieve sparse reconstruction and state extrapolation of full-state aerodynamic data for different aircraft shapes.

The main conclusions are as follows. SFL as a novel dimensionality reduction method for aerodynamic data, effectively generalizes across shapes. By extracting scaling functions from the historical aerodynamic data of typical aircraft, the scaling function expressions enable nonlinear dimensionality reduction in the aerodynamic parameter space. Using the SFL method, axial force scaling functions were extracted for HB-2. For new aircraft configurations, only 3 to 4 aerodynamic samples are required to optimize the scaling functions, enabling the construction of a full-state aerodynamic database and parameter extrapolation for the new shape. This demonstrates the excellent generalization and extrapolation capabilities of the extracted scaling function framework across different shapes and over a wide speed range, significantly reducing the cost of acquiring aerodynamic data for aircraft design.

Although the SFL method in this study was only applied to scaling aerodynamic coefficients for aircraft, SFL is a general framework for data dimensionality reduction, sparse reconstruction, and parameter extrapolation. In the future, the SFL method can be further applied to other complex high-dimensional engineering problems, providing robust support for dimensionality reduction and small-sample modeling in these parameter spaces.

## References

- [1] BRUNTON S L, NOACK B R, KOUMOUTSAKOS P. Machine learning for fluid mechanics [J]. Annual review of fluid mechanics, 2020, 52(1): 477-508.
- [2] TANG Z, ZHU L, XIANG X, et al. Some research progress and prospect of Intelligent Aerodynamics [J]. Acta Aerodynamica Sinica, 2023, 41(7): 1-35.

- [3] ZHANG W, KOU J, LIU Y. Prospect of artificial intelligence empowered fluid mechanics [J]. *Acta Aeronautica et Astronautica Sinica*, 2021, 42(4): 524689.
- [4] LI R, ZHANG Y, CHEN H. Transfer learning from two-dimensional supercritical airfoils to three-dimensional transonic swept wings [J]. *Chinese Journal of Aeronautics*, 2023, 36(9): 96-110.
- [5] WU H, LIU X, AN W, et al. A generative deep learning framework for airfoil flow field prediction with sparse data [J]. *Chinese Journal of Aeronautics*, 2022, 35(1): 470-84.
- [6] ZHANG W, PENG X, KOU J, et al. Heterogeneous data-driven aerodynamic modeling based on physical feature embedding [J]. *Chinese Journal of Aeronautics*, 2024, 37(3): 1-6.
- [7] PANG B, ZHANG Y, LI J, et al. Data-driven surrogate model for aerodynamic design using separable shape tensor method [J]. *Chinese Journal of Aeronautics*, 2024, 37(9): 41-58.
- [8] LUO C, HU Z, ZHANG S-L, et al. Adaptive space transformation: An invariant based method for predicting aerodynamic coefficients of hypersonic vehicles [J]. *Engineering Applications of Artificial Intelligence*, 2015, 46: 93-103.
- [9] CHEN J, ZHANG Y, ZHANG Y, et al. Review of correlation analysis of aerodynamic data between flight and ground prediction for hypersonic vehicle [J]. *Acta Aerodynamica Sinica*, 2014, 32(5): 587-99.
- [10] ARRINGTON J P, JONES J J. Shuttle Performance: Lessons Learned, Part 2 [R], 1983.
- [11] ZHANG Y, ZHANG Y, XIE J, et al. Study of viscous interaction effect model for typical hypersonic wing-body figuration [J]. *Acta Aerodynamica Sinica*, 2017, 35(2): 186-91.
- [12] KHRAIBUT A, GAI S L. Bluntness and incidence effects in hypersonic flows with large separated regions [J]. *JOURNAL OF FLUID MECHANICS*, 2022, 947: A5.
- [13] SHA X, CHEN X, JI F, et al. Study on Correlation of Aerodynamic Heating Data of a Combination Model [J]. *Procedia Engineering*, 2015, 99: 1604-09.
- [14] ŞAKRAKER I, TURCHI A, CHAZOT O. Hypersonic Aerothermochemistry Duplication in Ground Plasma Facilities: A Flight-to-Ground Approach [J]. *Journal of Spacecraft and Rockets*, 2015, 52(5): 1273-82.
- [15] RONCIONI P, LUIGI VITAGLIANO P, DE GREGORIO F, et al. Aerodynamic Appraisal of the VEGA-C Launcher [J]. *Journal of Spacecraft and Rockets*, 2023, 60(5): 1422-36.
- [16] LIU D W, XU X, WEI Z, et al. Engineering Extrapolation to Flight Reynolds Number for Supercritical Airfoil Pressure Distribution Based on CFD Results [J]. *Applied Mechanics and Materials*, 2013, 444-445: 517-23.
- [17] ÖZGÖREN A C. Reynolds number extrapolation for wind turbine airfoil polars: a data-driven approach [D]; Middle East Technical University, 2023.
- [18] MAKKE N, CHAWLA S. Interpretable scientific discovery with symbolic regression: a review [J]. *Artificial Intelligence Review*, 2024, 57(1): 2.
- [19] CORY-WRIGHT R, CORNELIO C, DASH S, et al. Evolving scientific discovery by unifying data and background knowledge with AI Hilbert [J]. *Nature Communications*, 2024, 15(1): 5922.
- [20] UDRESCU S-M, TEGMARK M. AI Feynman: A physics-inspired method for symbolic regression [J]. *Science Advances*, 2020, 6(16): eaay2631.
- [21] CRANMER M. Interpretable Machine Learning for Science with PySR and SymbolicRegression.jl [J]. 2023.

- [22] GUO S-Q, LIU W, ZHANG C-A, et al. Aerodynamic optimization of hypersonic blunted waveriders based on symbolic regression [J]. *Aerospace Science and Technology*, 2024, 144: 108801.
- [23] JIANG Z, LUO C. A Multi-space Interrelation Theory for Correlating Aerodynamic Data from Hypersonic Ground Testing [M]//SASOH A, AOKI T, KATAYAMA M. 31st International Symposium on Shock Waves 1. Cham; Springer International Publishing. 2019: 503-10.
- [24] SYED AHMED KABIR I F, GAJENDRAN M K, NG E Y K, et al. Novel Machine-Learning-Based Stall Delay Correction Model for Improving Blade Element Momentum Analysis in Wind Turbine Performance Prediction [J]. *Wind*, 2022, 2(4): 636-58.
- [25] CRANMER M. Pysr: Fast & parallelized symbolic regression in python/julia [J]. Zenodo, September, 2020.
- [26] CRANMER M, SANCHEZ GONZALEZ A, BATTAGLIA P, et al. Discovering symbolic models from deep learning with inductive biases [J]. *Advances in neural information processing systems*, 2020, 33: 17429-42.
- [27] KUCHI-ISHI S, WATANABE S, NAGAI S, et al. Comparative force/heat flux measurements between JAXA hypersonic test facilities using standard model HB-2 (Part 1: 1.27 m hypersonic wind tunnel results) [J]. JAXA research and development report, Japan Aerospace Exploration Agency, Japan, 2005.
- [28] VUKOVIĆ D, DAMLJANOVIĆ D. HB-2 high-velocity correlation model at high angles of attack in supersonic wind tunnel tests [J]. *Chinese Journal of Aeronautics*, 2019, 32(7): 1565-76.
- [29] ZHANG T, YE R, JIANG W, et al. Aerodynamic test data of hscm calibration models in hypersonic wind tunnel [J]. *Phys Gases*, 2021, 6: 57-65.
- [30] STEIN M. LARGE SAMPLE PROPERTIES OF SIMULATIONS USING LATIN HYPERCUBE SAMPLING [J]. *Technometrics*, 1987, 29(2): 143-51.
- [31] EAST R, HUTT G. Comparison of predictions and experimental data for hypersonic pitching motion stability [J]. *Journal of Spacecraft and Rockets*, 1988, 25(3): 225-33.
- [32] LI S. Typical hypersonic flow characteristics [M]. Beijing: National Defense Industry Press, 2007.
- [33] PRISLIN R. High amplitude dynamic stability characteristics of blunt 10-degree cones; proceedings of the 3rd and 4th Aerospace Sciences Meeting, F, 1966 [C].
- [34] DENG C, KONG Y, WANG Q, et al. Research on an Empirical Engineering Correction Algorithm Integrating Physical Laws [J]. *Air & Space Defense*, 2022: 73-79.